ELSEVIER

International Journal of Mass Spectrometry 220 (2002) 193–209

International Journal of Mass Spectrometry

www.elsevier.com/locate/ijms

Modelling ionic nucleation in small neon clusters

F. Sebastianelli [a], E. Yurtsever [b], F.A. Gianturco [a,*]

[a] *Citta Universitaria, Department of Chemistry and INFM, The University of Rome 'La Sapienza', 00185 Rome, Italy*
[b] *Department of Chemistry, Koç University, Istanbul, Turkey*

Received 12 October 2001; accepted 21 January 2002

Abstract

The structural properties of some of the smaller ionic clusters of neon atoms (Ne_n^+, $4 \leq n \leq 10$) are examined using different kinds of modelling for the interactions within each cluster. The results of the calculations, and the physical reliability of the methods, are discussed in comparison with earlier theoretical results and with experimental data. In spite of the simplicity of our model the present treatment is able to reproduce all the important features known for these clusters. (Int J Mass Spectrom 220 (2002) 193–209)

PACS: 36.40.+d; 34.20.−b

Keywords: Nucleation; Clusters; Modelling

1. Introduction

In the last years much attention has been paid to the rare gas ionic clusters Rg_n^+ from both the experimental and theoretical points of view [1–3]. All the studies so far suggest that these Rg_n^+ clusters consist of an arrangement of neutral, or almost neutral Rg atoms which are attracted by polarisation forces and, to a lesser degree, by dispersion forces to a charged central moiety Rg_k^+. The main problem is the size and structure of such ionic cores. Compared to He_n^+ and Ar_n^+, the number of papers dealing with Ne_n^+ clusters from a theoretical point of view are much fewer [4–9] and, furthermore, neon systems are less well studied experimentally than other rare gas clusters [10–13]. Even for the triatomic ion, Ne_3^+, the situation is not completely clear and, to the best of our knowledge, no experimental information of direct relevance for establishing its ground state geometry seems available at the moment. From the theoretical standpoint, the calculations investigating the Ne_3^+ features were performed using diatomics-in-molecules (DIMs) [5] and ab initio methods [4,6–9]. The DIM results of Kuntz and coworkers [5] predicted for the ground state geometry the T-shape configuration (C_{2v}) while the MRDCI results of Hogreve [6] the asymmetric linear one ($C_{\infty v}$). In both cases the charge is markedly delocalised (more than 90%) on the two neon atoms bound at a distance very close to that of the isolated Ne_2^+ molecule. The ab initio polarisation CI calculations of Wadt [4], the coupled clusters calculations of Naumkin and Wales [7] and the recent results of Urban et al. [9] performed by means of third-order multi-reference many body-perturbation theory (MR-MBPT) predict

* Corresponding author. E-mail: fa.gianturco@caspur.it

1387-3806/02/$ – see front matter
PII S1387-3806(02)00683-8

instead the linear symmetric configuration for the ground state with a more shared delocalisation of the charge over the three atoms. Larger clusters (Ne_n^+, $n > 3$) were studied using DIM methods [5,7] and with a DFT approach (the latter by us in a previous paper [8]). Although there are some differences in the results presented by those three papers about the energetics and the features of the structures found as the most stable ones, there is general agreement in stating that the ionic neon clusters, at least for the smaller aggregates, are built around a diatomic core on which nearly all the charge is localised. The remaining neon atoms are located either in the bisecting plane perpendicular to the dimer axis (up to five atoms), or further out in the apical positions along that axis. Our previous work on Ne_n^+ clusters, therefore [8] gave results in good agreement with the previous ones [5,7] although the computational effort required for a fully ab initio geometry and energy optimisations of larger size clusters, even at the DFT level, rapidly becomes prohibitive. In the present study we have therefore decided to examine instead the reliability of using an approximation to the global interaction between neon atoms inside the cluster given by the sums of pairwise potentials, as we shall describe in the next section. This treatment will allow us to make a comparison between the most stable structures we shall find with such an approach and the ones already present in literature. We could then use it as the starting point for the study of larger clusters, were the quality of this approach to be confirmed. In the following section we describe the computed anisotropic potential energy surface for the Ne_3^+ system and our approximation for the interaction forces, while in Sections 3–5 we present the method used for the optimisation, our final results and a comparison of them with earlier calculations and with an alternative model approach. Our final conclusions are then presented in Section 5.

2. The interaction forces

As mentioned earlier, all previous calculations found that in Ne_n^+ complexes the ionic core is given by a dimer ion with a distance between the two neon atoms practically identical to that of the isolated Ne_2^+ molecule. We therefore decided to model the global interaction potential within these clusters as sums of pairwise potentials, i.e. to approximate the full set of forces as the sum of the individual interactions between a Ne_2^+ and the relevant number of neon atoms, namely for a generic Ne_n^+ cluster, write

$$V_{\mathrm{TOT}}^{\mathrm{dimer}} = \sum_{i=3}^{n} V^{i}_{(\mathrm{Ne_2^+}-\mathrm{Ne})} + \sum_{\substack{i<j \\ i\geq 3}}^{n} V^{ij}_{(\mathrm{Ne}-\mathrm{Ne})} \qquad (1)$$

in which the first term is the sum of the interactions in the Ne_3^+ system considered as a rigid rotor, and the second term is the sum of the interactions between two neutral neon atoms. We therefore need to set up the relevant $V^{i}_{(\mathrm{Ne_2^+}-\mathrm{Ne})}$ and the $V^{ij}_{(\mathrm{Ne}-\mathrm{Ne})}$ interactions. For the calculation of the interaction which views Ne_2^+ as a rigid rotor system, we have used the DFT approach known as the Half & Half method of Becke (see [14] and references therein) in which the exchange-correlation energy is given in the form

$$E_{\mathrm{XC}} = E_{\mathrm{X}} + E_{\mathrm{C}}^{\mathrm{LSDA}} \qquad (2)$$

where E_{X} is the exchange energy of the Slater determinant of the final Kohn–Sham orbitals [15] and $E_{\mathrm{C}}^{\mathrm{LSDA}}$ is the local spin density approximation correlation functional. After a preliminary optimisation of Ne_2^+ molecule that gave a ground state distance of 3.276 a.u. (in good agreement with earlier findings [7–9]), we computed the potential energy surface (PES) for the Ne_3^+ system using the familiar Jacobi coordinates (see upper part of Fig. 1 for their definition), holding the molecular r coordinate fixed at the optimised distance of the Ne_2^+ isolated molecule and carrying out the calculations for 127 values of R (the distance between the centre of the dimer and the third neon atom) between 3.0 and 13.0 a.u. and seven values of the angle θ. For the long-range part of the potential we employed its polarisation tail by taking the experimental value of the dipole polarizability of the incoming Ne atom [16]. We can see from Fig. 1 the strong angular anisotropy shown by this PES: there is a deep minimum occurring for the collinear geometry

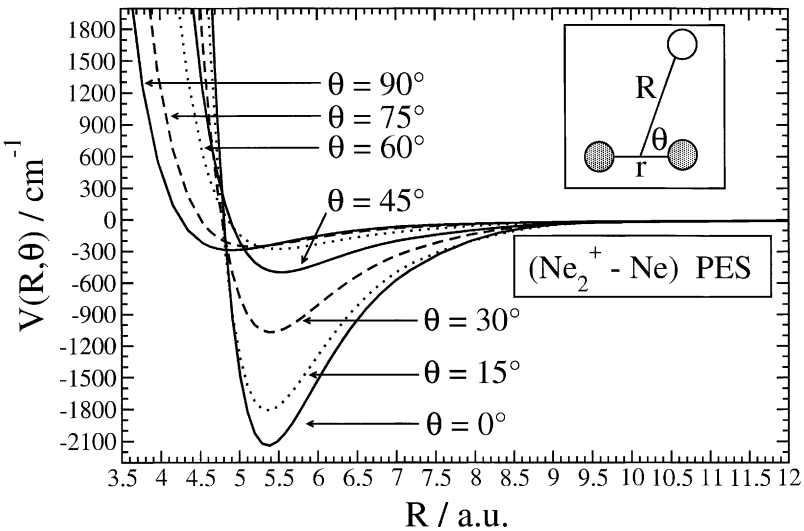

Fig. 1. The surface for the rigid rotor Ne_3^+ system: the computed curves for the seven different angles are shown. In the upper panel the Jacobi coordinates are presented.

($\theta = 0^\circ$), corresponding to the asymmetrical linear trimer, and a shallow minimum corresponding to the T-shape arrangement ($\theta = 90^\circ$). For the Ne–Ne neutral interaction ($V^{ij}_{(\mathrm{Ne-Ne})}$ in Eq. (1)) we used the accurate interatomic potential given by Kleinekathöfer et al. [17] based on the Tang–Toennies model [18]. To further extend our comparison, we also decided to model the total interactions in an alternative way, i.e. using only atomic potentials with an ionic atomic core in order to see how well the results appear to describe the final ionic clusters in this simplified picture. Therefore, the total potential of this set of calculations was given as

$$V^{\mathrm{atomic}}_{\mathrm{TOT}} = \sum_{i=2}^{n} V^{i}_{(\mathrm{Ne^+-Ne})} + \sum_{\substack{i<j \\ i\geq 2}}^{n} V^{ij}_{(\mathrm{Ne-Ne})} \qquad (3)$$

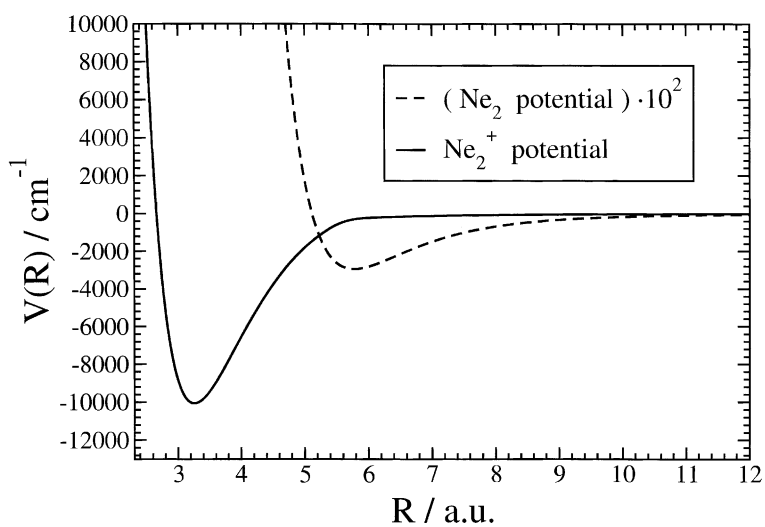

Fig. 2. The potential energy curves for Ne_2 and Ne_2^+. The Ne_2 potential is magnified by 10^2.

where the first term on the RHS is the interaction potential for isolated Ne^+–Ne and the second one is the same neutral interaction as in Eq. (1). We computed the $V^i_{(Ne^+-Ne)}$ part of Eq. (3) using an accurate one-dimensional potential curve within the coupled cluster theory, choosing single and double excitations (CCSD). We show this curve in Fig. 2, where we also report the Ne_2 potential, magnified by a factor of 10^2 in order to have both curves on the same plot.

3. The optimisation procedures

Having set up all the necessary interaction potentials, the next task is to employ them for the geometry and total energy optimisation process. First of all, we rewrite the $V^i_{(Ne_2{}^+-Ne)}$ potential via the usual Legendre angular expansion

$$V^i_{(Ne_2{}^+-Ne)} = V(R,\theta) = \sum_{\lambda=0}^{12} V_\lambda(R) P_\lambda(\cos\theta) \qquad (4)$$

where λ will take only even values due to the symmetry of the system. We then employed a simple steepest descent algorithm that makes use of the $V^{\text{dimer}}_{\text{TOT}}$ as given in Eq. (1). In this case (which we shall call from now on the 'dimer–atom (D–A) optimisation' for the sake of brevity) we hold fixed the $Ne_2{}^+$ bond distance and we leave out from the calculations the first two atoms which will constitute the charged core and are positioned midway along the z axis as in Fig. 3. We use a cubic spline for the $V^{ij}_{(Ne-Ne)}$ terms of Eq. (1) in order to have an analytical representation of the

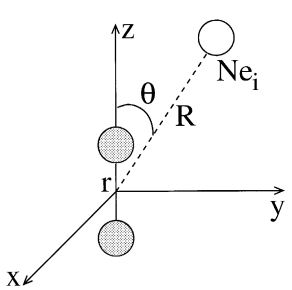

Fig. 3. The orientation of the dimer core with respect to the Cartesian coordinates system used in our calculations.

dimer–atom potential, and write down the first derivatives of $V(R,\theta)$ in Cartesian coordinates

$$\frac{\partial V}{\partial x_i} = \frac{\partial V}{\partial R}\frac{\partial V}{\partial x_i} + \frac{\partial V}{\partial \cos\theta}\frac{\partial \cos\theta}{\partial x_i} \qquad (5)$$

where

$$\frac{\partial V}{\partial x_i} = \frac{x_i}{R}\sum_\lambda P_\lambda(\cos\theta) V'_\lambda(R) - \frac{x_i z_i}{R^3}\sum_\lambda P'_\lambda(\cos\theta) V_\lambda(R) \qquad (6)$$

As input geometries in the calculations we take all the structures obtained from our previous work, both local minima and global minima, and the optimised geometries of Naumkin and Wales [7] (called from now on the 'DIM structures') which will be analysed in detail in the next section. The ones previously found by us [8] will be called the full ab initio potential structures, as discussed in the next section. The structures optimised with the latter method will be further compared with the ones we have obtained via the alternative optimisation method given by the OPTIM code by Wales (see [19] and references quoted therein for a complete discussion of the method) implemented by us for our potential, and using the potential first and second derivatives in Cartesian coordinates required to yield the analytical expression of the Hessian. The method is basically an eigenvalue following method which is particularly suited for multi-dimensional potential landscapes that contain several shallow basins as is the case here. The structures we computed using both procedures are found to be nearly identical to the previous ones so that combining the two different optimisation methods assure us of a better consistency of our results. We also observed that the energies for the structures found with the OPTIM code are always lower than those ones obtained with our steepest descent algorithm. Even much clearer is the situation for the optimisation using the $V^{\text{atomic}}_{\text{TOT}}$ global potential (from now on the 'atom–atom (A–A) potentials optimisation'): the steepest descent algorithm is very sensitive to the initial geometries and very different structures are obtained when starting with different input arrangements, while the use of OPTIM always yields the same

structures (and always lower in energy) regardless of the initial geometries. Such results are not really surprising as the steepest descent methods are known to often fail for interaction potential situations as those we are analysing here. Therefore, in the next sections we will show only the geometries we found using the OPTIM method and will discuss in detail the features of these structures, comparing them with previous findings.

4. Analysis of results

4.1. The optimised structures

Before starting to examine our results we need to provide a general overview of the features of the Ne_n^+ structures studied so far from a theoretical standpoint [5,7,8]. The main differences between the results of Naumkin and Wales [7] and the findings in [5,8] (for Ne_n^+ with $4 \leq n \leq 10$), are with the clusters up to Ne_7^+. Referring to Fig. 4, in which a general cluster is taken as an example, we can talk about a process of filling shells in competition with each other, where the almost neutral neon atoms (three in Fig. 4) located in the plane bisecting perpendicularly the dimer core axis are in the first shell, while the neon atoms in the apical positions (two in Fig. 4) are taken to be in the second shell. In the work described in [7] the global minimum structures are those in which one finds the presence of a linear tetrameric unit (basically the lowest optimised geometry for the Ne_4^+ cluster) around which the other neon atoms start to locate themselves until they have filled the first shell (Ne_9^+, with five neon atoms in the perpendicular plane). For all these clusters the tetrameric unit is always present (up to $n = 10$) as it can be seen in the upper panels of Figs. 5–7 where we report the findings of Naumkin and Wales [7]. On the other hand, the results obtained in [5,8] are quite similar with each other in that they found the most stable structures to be the ones in which the perpendicular plane is filled at first (Ne_4^+ to Ne_7^+) and then the second shell starts to be filled (Ne_8^+ to Ne_{10}^+). The results of [8] are shown on the lowest panels of Figs. 5–7. Although we refer to [8] for a more detailed discussion of these results, we just want to stress here that the structures which in one case [7] are found as local minima are in the other case [8] the global minima and vice versa (see upper and lower panels in Figs. 5 and 6), while for the larger clusters in Fig. 7, we see that both the top and bottom panels yield similar structures as global minima. The results become therefore the same for Ne_8^+, Ne_9^+ and Ne_{10}^+, as clearly seen there. If we now use all the findings as input for the dimer–atom optimisation mentioned before, we obtain the results shown in the middle panels of Figs. 5–7. With the modelling of the full interaction potentials we therefore get results similar to those of [7], i.e. the most stable structures show the presence of the tetrameric unit up to Ne_7^+, and the remaining clusters ($8 \leq n \leq 10$) show structures in good agreement with the previous findings. In Fig. 8 we further show what we found for the optimisation procedures in which the atom–diatomic total potential is given for $4 \leq n \leq 7$ and compared with the full, ab initio optimisation procedures. One clearly sees that the local minima provided by the ionic dimer core modelling are very similar to the actual global minima given by the total optimisation procedure, a point which we shall further elaborate on in the following discussion. If we now compare the findings with the global minima which are produced by using

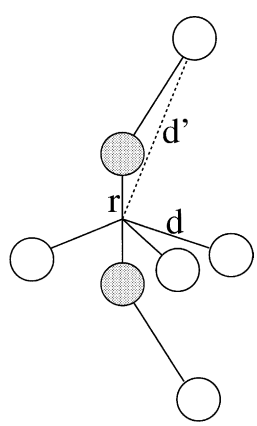

Fig. 4. A generic Ne_n^+ cluster with the distance parameters used in the calculations and discussed in the main text.

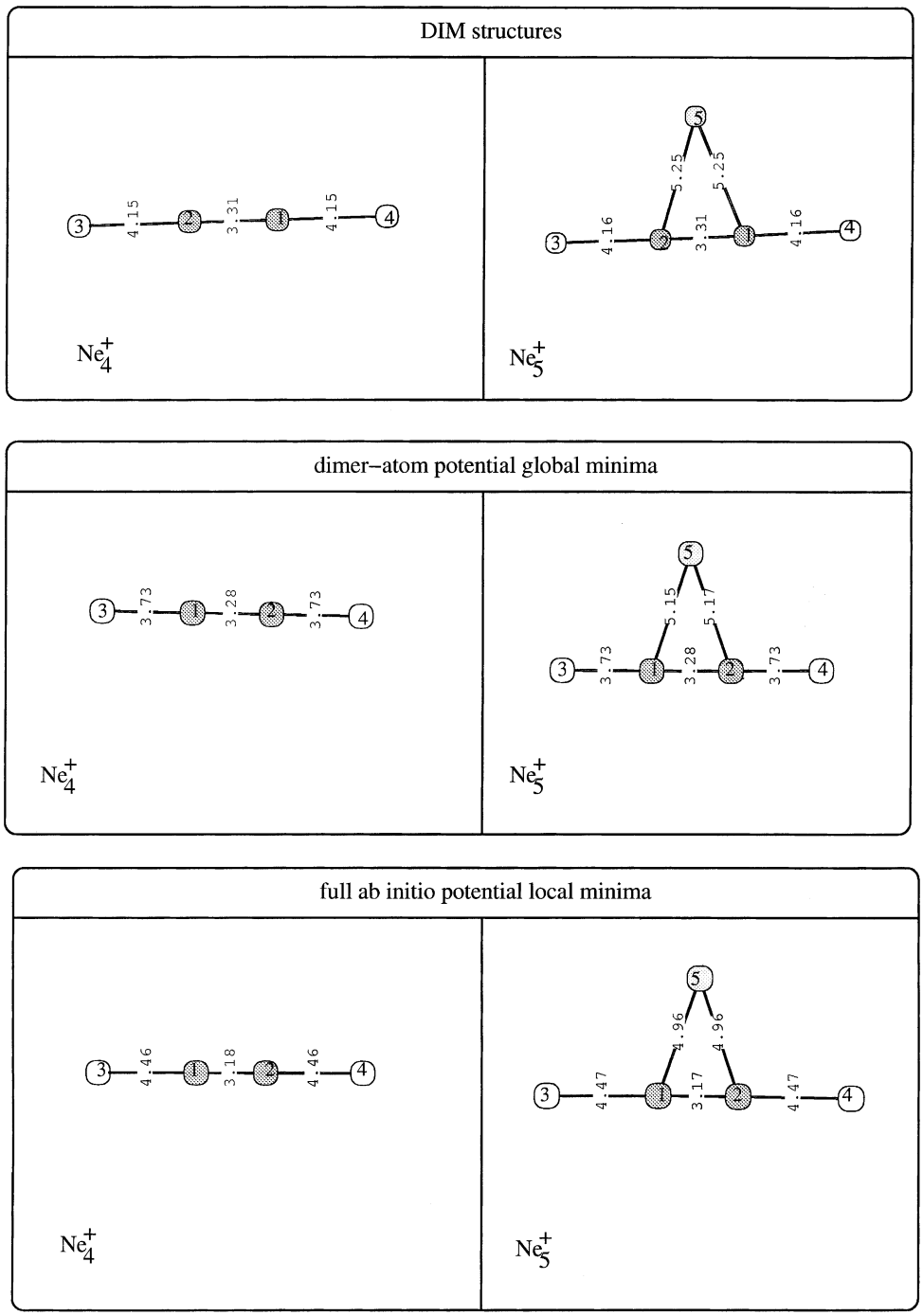

Fig. 5. Ne_4^+ and Ne_5^+ clusters: in the middle panel we report the present results.

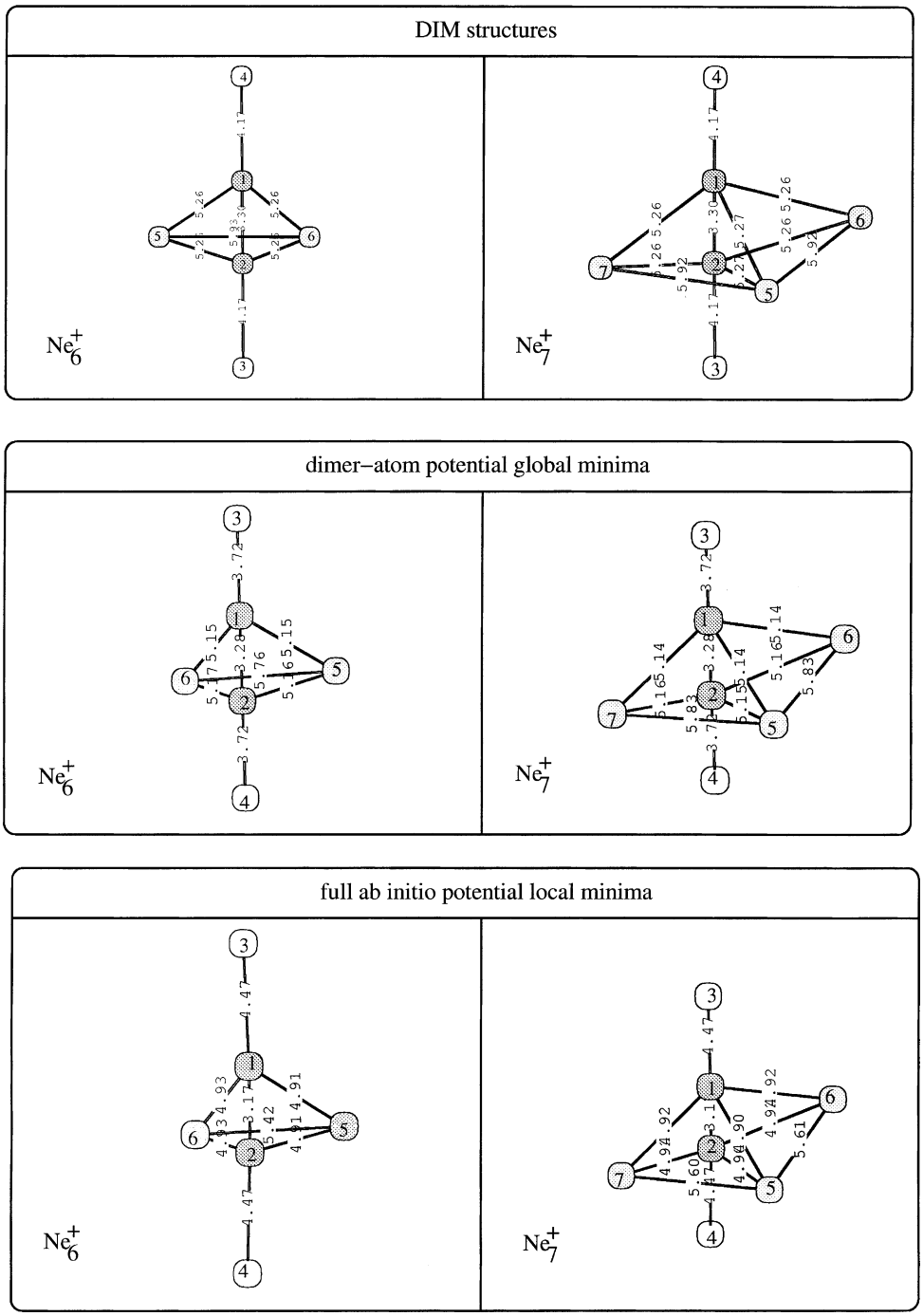

Fig. 6. Ne_6^+ and Ne_7^+ clusters. Middle panel: dimer–atom global minima. Also shown the DIM structures [7], upper panel, and the local minima obtained in [8].

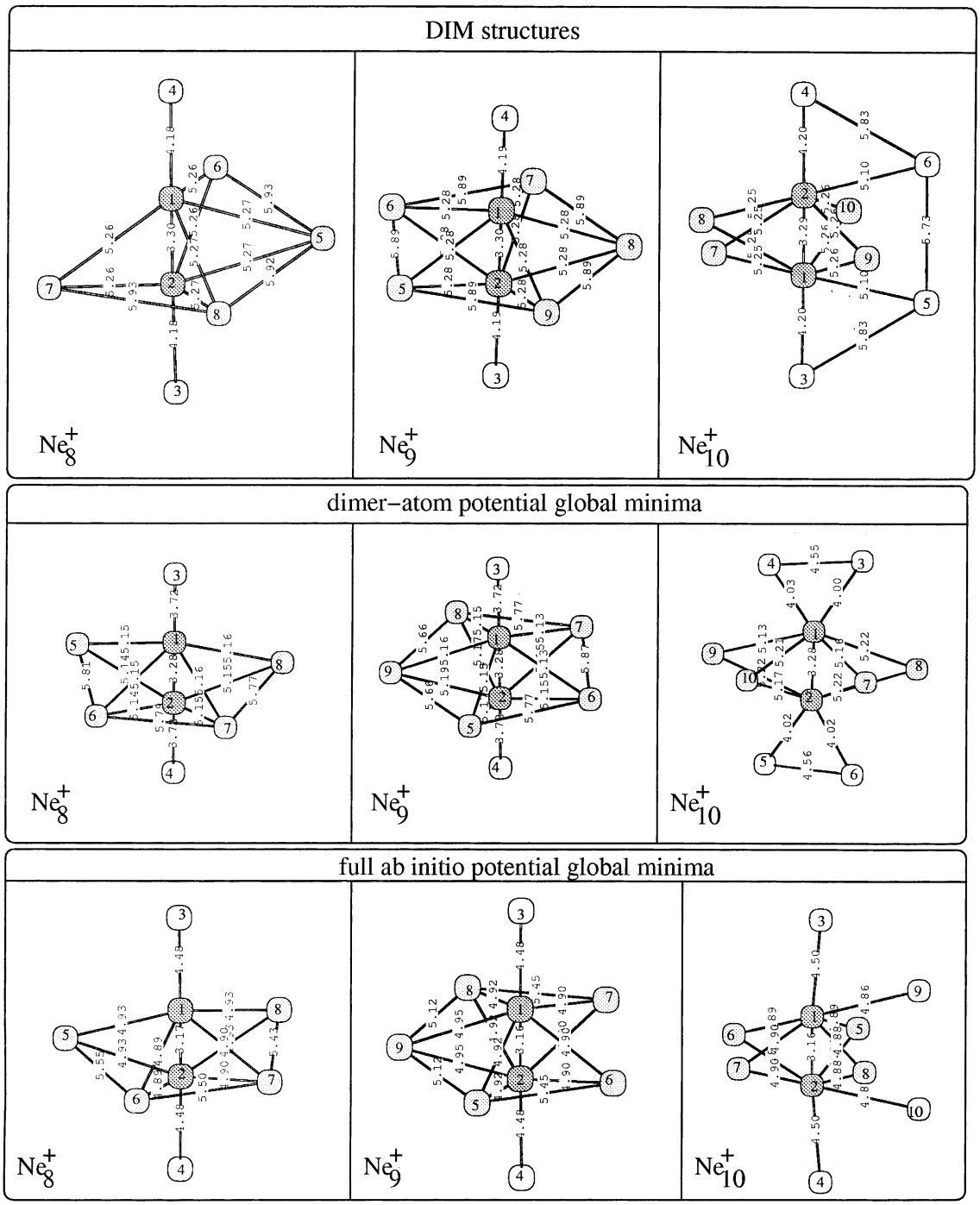

Fig. 7. Ne_8^+–Ne_{10}^+ clusters. Middle panel: present results.

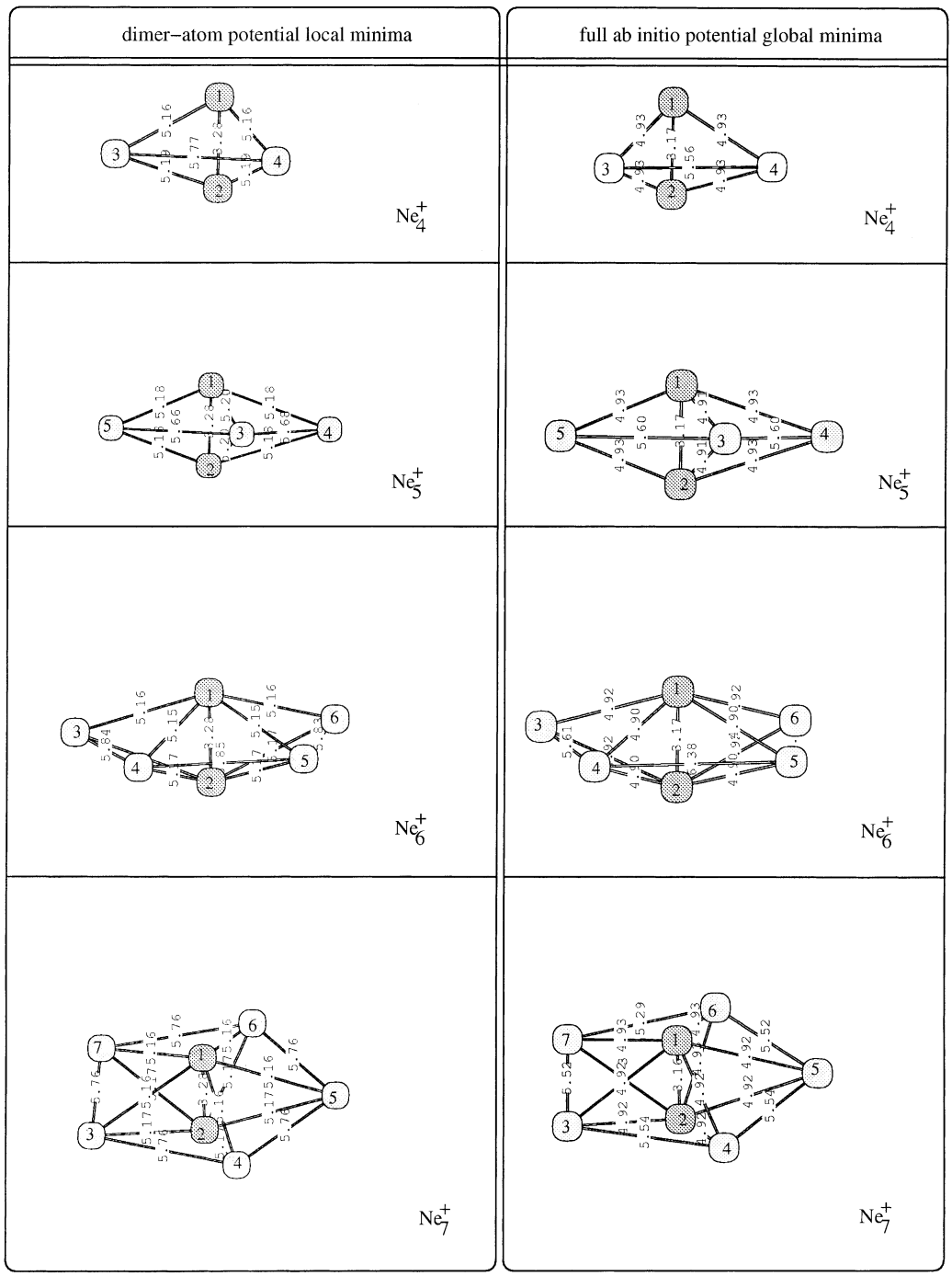

Fig. 8. Ne_4^+–Ne_7^+ local minima obtained here and, on the right, the full ab initio potential global minima [8].

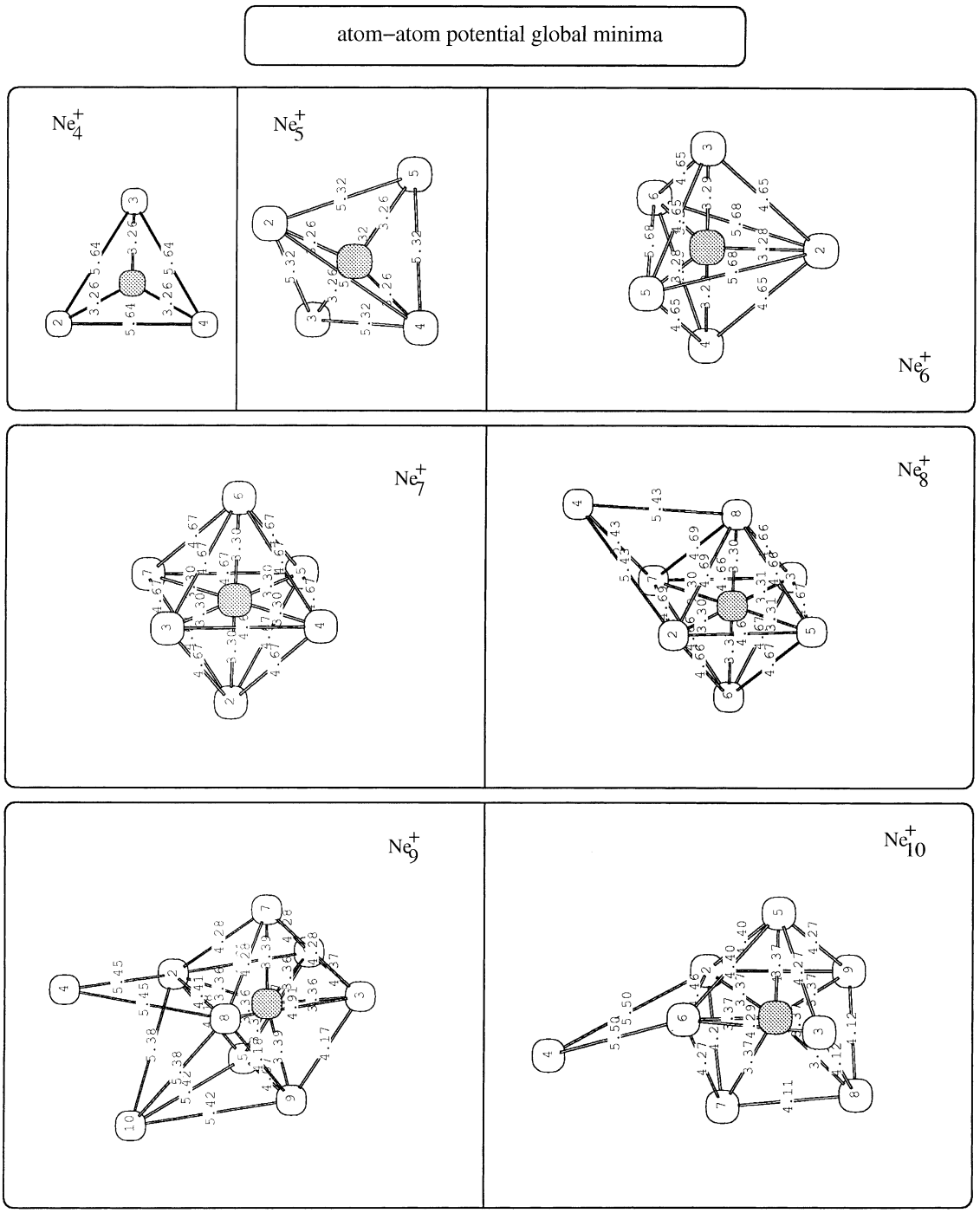

Fig. 9. Structures found for atomic potentials modelling of the global interactions.

the atom–atom model, it appears immediately evident (see Fig. 9) that the atomic modelling brings structures completely different from all the ones already discussed and obtained either by global optimisation of the clusters or by assuming an ionic core at their centres. In the following we will try to analyse the similarities more in detail and try to extract from our calculations further indicators for the evaluation of the cluster features.

4.2. Further comparative features

Having discussed all the minimum energy structures found within our modelling of the global interactions as given by Eqs. (1) and (3), we proceed next to a systematic comparison between our findings and the previous results [7,8]. In Fig. 10 we report the relevant distances which help us to characterize the shape of the clusters, plotted as a function of the cluster size. The results are those obtained by employing the dimer–atom potential. As presented in Fig. 4, d is the distance between the centre of the dimer core and each neon atom located in the perpendicular plane, a parameter which helps us to define the first shell. The d' is the distance between the centre of the dimer core and each of the neon atoms located in an apical position. It helps us to label the second shell of solvent atoms surrounding the ionic core. In Fig. 10 we further report $\bar{d}$ and $\bar{d}'$, which here represent the mean values of the already defined distances within each particular cluster. The r's represent the values of the bond distance in each ionic core along the series of clusters, a parameter seen to be markedly smaller than any other distance between partner adatoms. We further show for comparison, in Fig. 11, the corresponding quantities obtained from our previous calculations, where we used the full ab initio potential optimisation [8]. One sees clearly there that the shell pattern features are substantially maintained and semiquantitative agreement is achieved between the results from the two methods. In Fig. 10 the r distance is reported just for completeness as it was kept fixed in the calculations, where we have left this degree of freedom frozen to its value for the isolated Ne_2^+ molecule. The main difference between the two sets of calculations given by Figs. 10 and 11 is that the structures obtained with the model potential are somewhat more compact, that is in each of the clusters the d' values are closer to the d values. We cannot make a significant comparison for

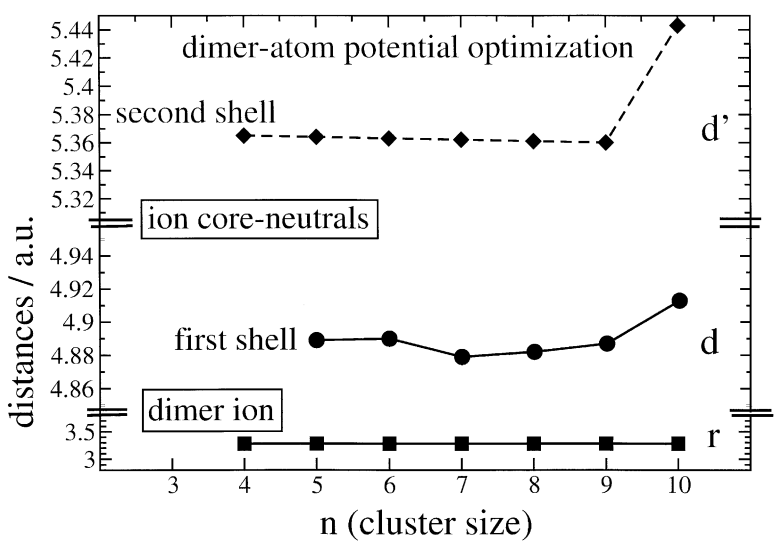

Fig. 10. Average distances of the global minimum structures (from Ne_4^+ to Ne_{10}^+) from dimer–atom model optimisations. The distance of the dimer core was held fixed (3.276 a.u.).

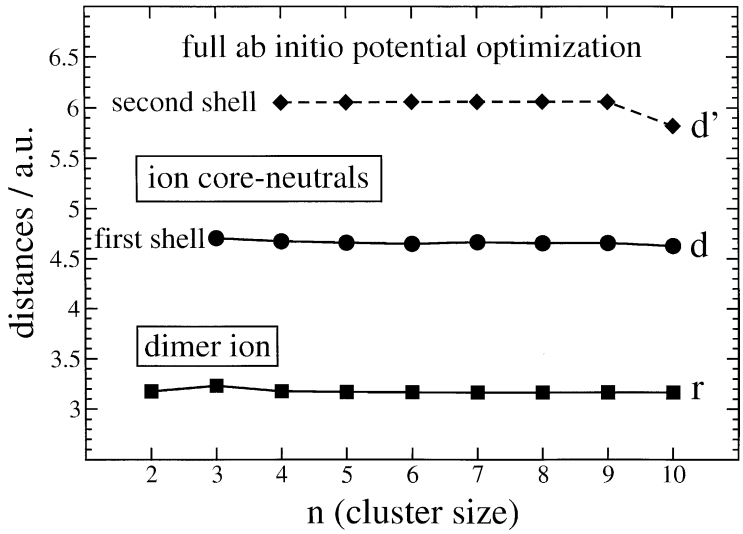

Fig. 11. Average distances from ab initio optimisations, see [8].

the geometries obtained with atom–atom potential modelling since the latter structures lack a similar shell structure, as shown by Fig. 9, and are very different from those just discussed. We can argue that the driving force in the last case acts to locate as many neon atoms as possible at a distance near to the equilibrium value for Ne_2^+ (about 3.3 a.u.), a tendency balanced only by the residual repulsive interactions between each other. We see therefore that with the Ne_7^+ cluster this special first shell is completed. As a consequence of it, the Ne_8^+ to Ne_{10}^+ structures (middle and lower panels of Fig. 9) are not nearly as symmetric as the previous ones and it is therefore difficult to discern a second shell when only the atom–atom potentials are employed. On the other hand, we have found here that the results obtained via the dimer–atom potential modelling give final geometries, for the lowest energy structures, in agreement with the findings of [7], although slightly different from what we had found earlier [8] using a full ab initio potential. Hence, an additional type of comparison can be made by now looking at the behaviour of their corresponding moments of inertia and doing it for all the optimised structures. We report these results in Figs. 12 and 13. In order to make a comparison which shows more clearly relative changes, the moments of inertia are normalised to the largest one, i.e. if $I_a < I_b < I_c = I_{max}$, then we take

$$I'_a = \frac{I_a}{I_{max}} \tag{7}$$

and

$$I'_b = \frac{I_b}{I_{max}} \tag{8}$$

In Fig. 12 we report I'_a (upper part) and I'_b (lower part) as a function of the cluster size for the structures in which we found the presence of the linear tetrameric unit, and for the geometries obtained with atom–atom potential modelling (square symbols): in the case of the results obtained via the dimer–atom potential the values of the moments of inertia are seen to be quite similar with the findings of [7,8]. On the other hand, the results obtained via the atomic potentials are very far from the others. The same analysis, given by Fig. 13, can be made for the structures in which the neon atoms first locate themselves in the perpendicular plane. The agreement between the dimer–atom potential and the full ab initio optimisations is quite good. As a further demonstration of the reliability of using the atom–diatom interaction model, we show in Fig. 14 the single atom evaporation energies plotted as a function of the cluster size. The experimental values

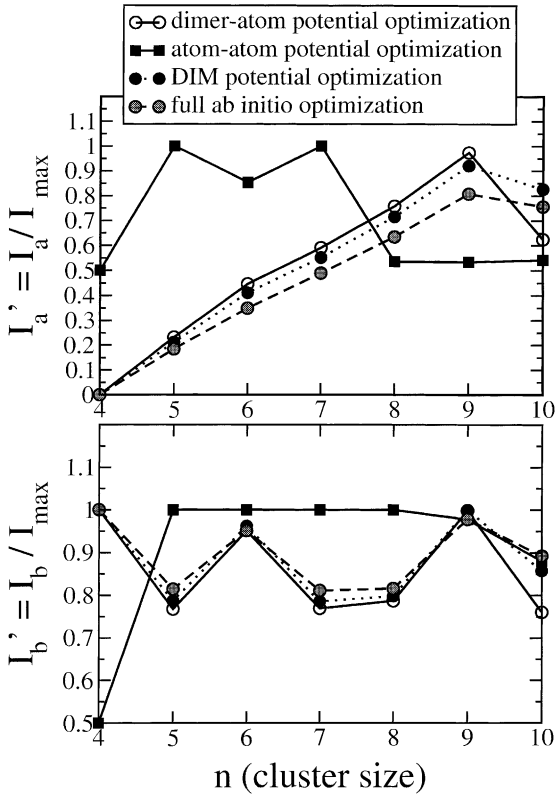

Fig. 12. Comparison between 'normalised' momenta of inertia of the present results with those from the configurations of [7,8].

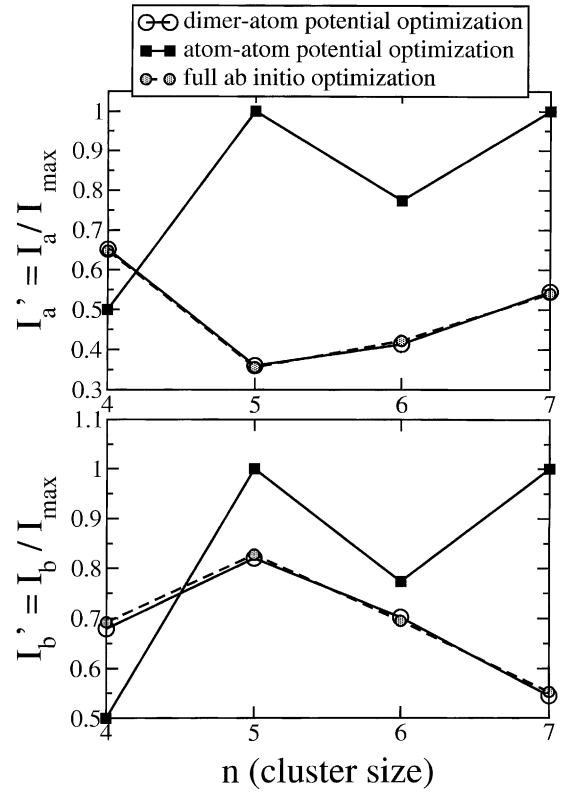

Fig. 13. Comparison between 'normalised' momenta of inertia of local minima from present results with those from the configurations of [8].

given by open, unconnected circles are from [10] while the filled-in circles without connecting lines are from [20]. Within the calculations, the main difference which we now see is the reduced effect of magic numbers for the DIM optimisation, in the sense that this approximation cannot detect the sudden changes in the energy values for $n = 10$ as shown by both the ab initio optimisation [8] and the dimer–atom potential of present work. The fact that the sudden variation of the evaporation energies at $n = 10$ shows opposite sign between the ab initio and the atom–diatom potential results could be attributed to the fact that the latter modelling favours the dimeric core, thereby increasing the energy required to evaporate one atom with respect to the case where a tetrameric core is present (see Fig. 7). A comparison of the calculations with the two sets of experimental data shows that all of them fall between the two measurements: the data of [10] suggest an average value of about 32 meV for $5 \leq n \leq 9$ while the newer data of [20] indicate a much more structured behaviour which suggests an average of 60 meV per atom. Our calculations with the ab initio methods show the most structured data and all calculations indicate an average value of about 45 meV per atom.

Another point of interest could be to analyse the range of the differential energetics with the various potentials employed to analyse the small cluster structures. For this purpose, we report in Fig. 15 the comparative behaviour of the ionic clusters with $4 \leq n \leq 7$, obtained using the dimer–atom interaction model (upper panel) and the full ab initio potential (lower panel). The energy values shown there are given in units of meV and correspond, for each n value, to the

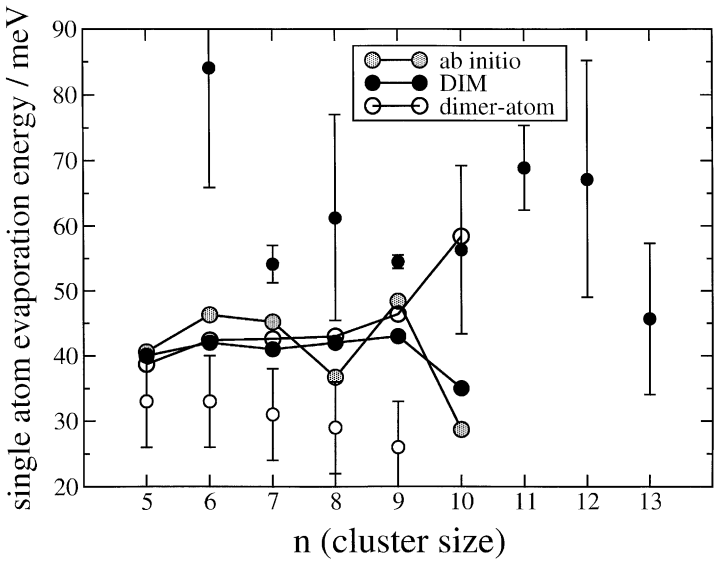

Fig. 14. Comparison of the single atom evaporation energies obtained from the different calculations. The experiments are given by the unconnected open circles [10] and by the unconnected filled circles (from [20]).

modulus of the difference between the energy of the local minimum structure and that of the corresponding global minimum structure. The dimer–atom results consistently show that the global values are lower than the local ones by an energy range which is about three orders of magnitude larger than the range existing for the ab initio potential calculations. Hence, it is fair to say that the interchange of cluster shapes seen before when going from the model potential results to the ones from the ab initio potentials are mainly due to the existence of a smoother potential energy landscape produced by the latter calculations in comparison with that given by the former. In the case of the model potential, therefore, local configurations get locked-in much more efficiently by its more strongly "corrugated" energy landscape given by the use of the addition of analytic potentials chosen in Eq. (1).

4.3. The polygon growth model (PGM)

What we have found through the previous analysis is a general agreement between various calculations on the fact that a dimeric ionic core is at the centre of the network of neon atoms. Furthermore, our calculations indicate that, at least for the smaller clusters, the growth occurs by the addition of a finite number of Ne atoms either around the dimer axis or at the two apical ends of it. It therefore becomes of interest to see what information could be gathered if we were to create an even simpler modelling of the interatomic forces within the cluster based on the findings. In the following we will describe and analyse the outcome of using a simplified interaction which we shall call the polygon growth model (PGM). In this approach, a core of two atoms and a positive charge is located along the z Cartesian axis of the cluster. The neutral adatoms are then gathered in a number of polygons with equal sides that are placed as perpendicular to the dimer core z axis, as depicted in Fig. 16. Their geometry is therefore defined by: (i) the distance of each polygon's centre from the origin of the z axis, d_p, and (ii) the radius of the polygon, r_p. The interactions between the neutral atoms of each polygon use the atom–atom neutral potential discussed before, while the interactions of those atoms with the ionic core employ our diatom–atom potential as described earlier. The structural energies can then be computed for each $\{r_p, d_p, n\}$ set of values. To begin with, we only look

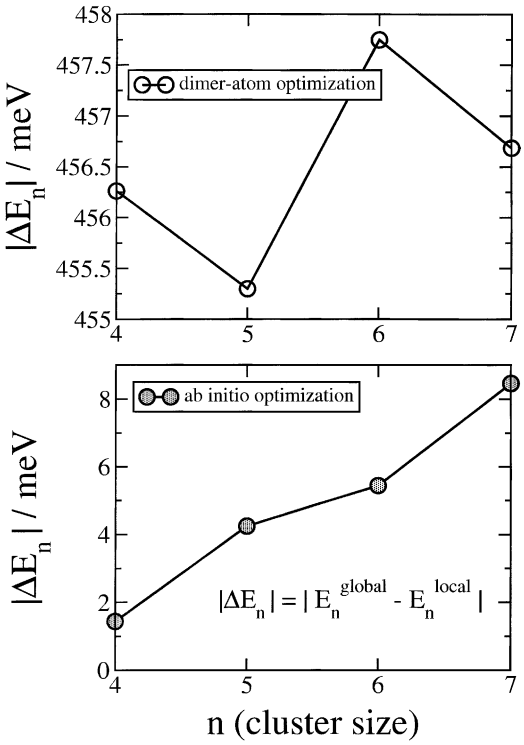

Fig. 15. Modulus of the energy differences between local and global minima for the two different optimisation processes discussed in the main text.

here at the systems with one polygon. Since two atoms are already used for the core, n represents now only the number of neutral atoms and therefore any given n corresponds to an Ne_{n+2}^{+} cluster. For each d_p value, the corresponding radius r_p is optimised with respect to the total energy, to find the global minimum energy structures. The results of Fig. 17 show the behaviour of the total energy, in units of E_{min}/n to make the comparison easier, as a function of the polygon distance from the centre of charges and for the number of atoms in each polygon varying from $n = 2$ up to $n = 12$. The data in Fig. 18 report the optimum sides of the polygon, as a function of d_p, and for the same set of n values. A combined perusal of the results allows us to state the following:

(i) the stabilisation energy of the polygon decreases dramatically when more adatoms appear in it and, when n reaches beyond five atoms, it becomes a very smooth function of the d_p value, reaching its optimum stabilisation when $d_p = 0$, which is what the previous, more complex calculations had found;
(ii) when the optimised radii are transformed into length of sides of each polygon, the data show that, after $n = 5$, all clusters tend to form polygons where the neutral–neutral distance remains around 5.7 a.u. and the optimisation is best when d_p goes to zero;
(iii) small clusters up to $n = 5$ (Ne_7^{+}) are relatively the most stable clusters and their distances to the centre of charges are optimised around 4.5 a.u., remarkably close to the results of the previous section.

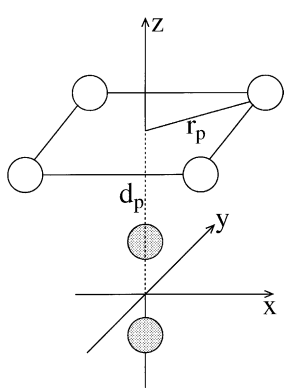

Fig. 16. Parameters characterising the polygon growth model (PGM).

Thus, it seems that this simple model is already providing confirmation of specific features of the more complex calculations, e.g. (i) the first shell is in the middle of the dimer core and orthogonal to its axis, (ii) the optimum size of it is with five atoms and (iii) its best size is that which keeps adatoms at a relative distance from the z axis of about 4.5 a.u. We are currently extending it to larger systems[1] with a larger number of polygons, finding that the latter shapes indeed contain an optimum number of adatoms beyond which the next polygon starts to be filled in. In other words, we see the clusters growing along a preferential growth

[1] F.A. Gianturco, E. Yurtsever, F. Sebastianelli, in preparation.

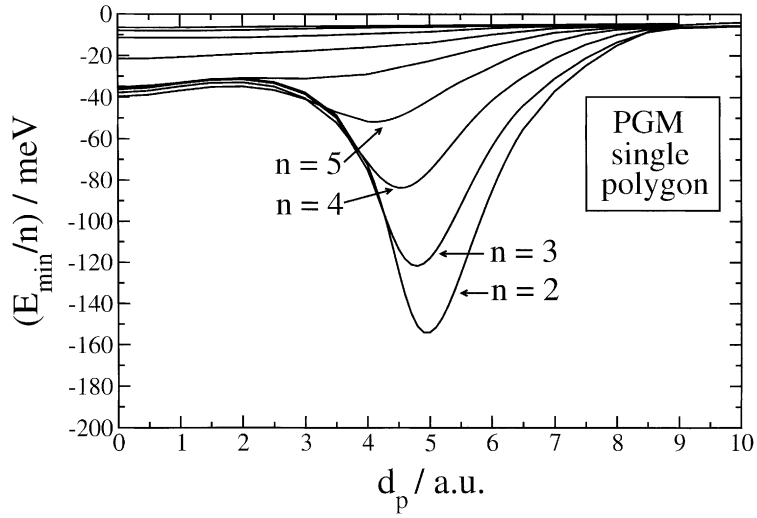

Fig. 17. Total energy, in units of E_{min}/n, as a function of the polygon distance from the centre of charges and of the number of atoms in each polygon varying from $n = 2$ to $n = 12$.

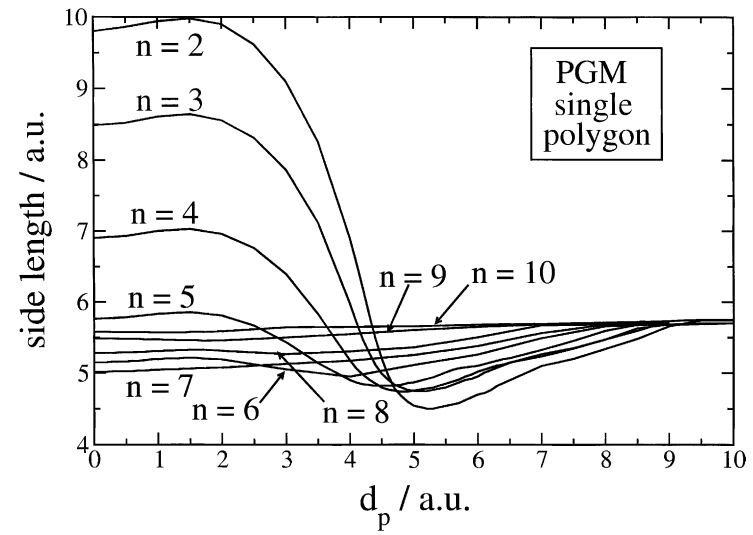

Fig. 18. Optimum sides of the polygon, as a function of d_p, and for the same set of n values as in Fig. 17.

axis defined by the charged dimer core instead of following the more spherical growth of neutral clusters.

5. Conclusions

With the work described in the previous sections we have analysed the most likely structures of ionised neon clusters up to 10 atomic partners. We had discovered already from previous calculations [5,7,8] (which used different methods for constructing the full interaction) the presence of a dimeric ionic unit where the great majority of the charge is localised. We therefore decided to model the full interaction in a way that could realistically resemble this feature by choosing the full potential as a sum of Ne_2^+–Ne

and Ne–Ne interactions. The qualitative picture that emerges from our calculations allows us to draw the following conclusions:

1. The most stable structure for Ne_4^+ is the linear one with the other two neon atoms positioned at a distance of about 5.4 a.u. from the centre of the dimer core, that is the first two atoms locate themselves in the second shell.
2. The successive positioning of further neon atoms (Ne_5^+ up to Ne_9^+), for the most stable structures, begin in the bisecting plane perpendicular to the dimer core, i.e. the first shell starts to be filled until there are five neon atoms in this plane (the maximum possible value for balancing the repulsion forces between two neon atoms).
3. With the two biggest clusters which we are considering here, Ne_9^+ and Ne_{10}^+, we see that a second shell along dimer axis direction and higher up from the charges gets to be filled with four neon atoms.
4. The atom–atom potential modelling, see Eq. (3), brings on the other hand very different sets of geometries, as one should aspect. It seems important, in fact, to at least take into account of the anisotropic interaction between a molecular core, Ne_2^+, and the neutral neon atoms added to that core.

The defined considerations are in line with what has been found before [7] where, however, the presence of a tetrameric unit in the smaller clusters was surmised. This was partly in contrast with our previous findings [8], where however we did not use a model potential like in the DIM approach but rather an all-electron treatment within a DFT formulation. The structures we found in [8] turned out to be local minima over a rather smooth potential energy landscape and therefore energetically not far from the global minima given by [7]. However, and this is an important point, we also found that starting from the Ne_8^+ cluster all the different approaches essentially merge in the sense that all suggest the dimeric unit as the core for the larger Ne_n^+ clusters. It therefore follows that to employ the present Ne_2^+–Ne potential modelling provides a reasonable starting point for studying larger clusters for which a full ab initio optimisation is currently outside the range of computational capabilities and which can thus be obtained using the present approach. This analysis is the subject of the work presently in progress in our group (see footnote 1).

Acknowledgements

The financial support of the Italian Ministry for University and Research (MURST) and the CASPUR computing Consortium is here acknowledged. We are also grateful for a collaborative research grant awarded within the CNR (Italy)-TUBITAK (Turkey) Scientific agreement for the year 2000–2001.

References

[1] H. Haberland (Ed.), Clusters of Atoms and Molecules, Springer, Berlin, 1994.
[2] C.Y. Ng, T. Baer, I. Powis (Eds.), Cluster Ions, Wiley, New York, 1993.
[3] I. Last, T.F. George, J. Chem. Phys. 93 (1990) 8925.
[4] W.R. Wadt, Appl. Phys. Lett. 38 (1981) 1030.
[5] M. Fieber, A.M.G. Ding, P.J. Kuntz, Z. Phys. D 23 (1992) 171.
[6] H. Hogreve, Chem. Phys. Lett. 215 (1993) 72.
[7] F.Y. Naumkin, D.J. Wales, Mol. Phys. 93 (1998) 633.
[8] F.A. Gianturco, F. Sebastianelli, Eur. Phys. J. D 10 (2000) 399.
[9] J. Urban, P. Mach, J. Mášik, I. Hubač, V. Staemmler, Chem. Phys. 255 (2000) 15.
[10] K. Hiraoka, T. Mori, J. Chem. Phys. 92 (1990) 4408.
[11] T.D. Märk, P. Scheier, Chem. Phys. Lett. 137 (1987) 245.
[12] M. Fieber, G. Broker, A. Ding, Z. Phys. D 20 (1991) 21.
[13] T.D. Märk, P. Scheier, J. Chem. Phys. 87 (1987) 1456.
[14] A.D. Becke, J. Chem. Phys. 98 (1993) 1372.
[15] R.G. Parr, W. Yang, Density Functional Theory of Atoms and Molecules, Oxford University Press, Oxford, 1989.
[16] J. Leonard, At. Data Nucl. Tables 14 (1974) 21.
[17] U. Kleinekathöfer, K.T. Tang, J.P. Toennies, C.L. Yiu, Chem. Phys. Lett. 249 (1996) 257.
[18] K.T. Tang, J.P. Toennies, J. Chem. Phys. 80 (1984) 3726.
[19] D.J. Wales, J. Chem. Phys. 101 (1994) 3750.
[20] R. Parajuli, S. Matt, O. Echt, A. Stamatovic, P. Scheier, T.D. Märk, Chem. Phys. Lett. 352 (2001) 288.